Metal Halide Perovskite and Perovskite–like Materials Through the Lens of Ultra–wideline $^{35/37}$Cl NMR Spectroscopy

Diganta Sarkar,[a] Riley W. Hooper,[a] Abhoy Karmakar,[a] Amit Bhattacharya,[a] Arkadii Pominov,[a] Victor V. Terskikh,[b] and Vladimir K. Michaelis*,[a]

[a]Department of Chemistry, University of Alberta, Edmonton, Alberta T6G 2G2, Canada
[b]Metrology, National Research Council of Canada, Ottawa, Ontario K1A 0R6, Canada

Corresponding author: vladimir.michaelis@ualberta.ca

ABSTRACT

With their exceptional optoelectronic features, metal halide perovskites (MHPs) are pushing the next wave of energy–related materials research. Heretofore, most solid–state nuclear magnetic resonance (NMR) investigations have focused on readily accessible nuclei. In contrast, the halogen environments have been avoided due to their challenging quadrupolar nature. Here, we report a rapid $^{35/37}$Cl NMR strategy for MHPs, halide double perovskites (HDPs) and perovskite–inspired (PI) materials embracing ultra–wideline acquisition approaches at moderate and ultrahigh magnetic fields. The observed quadrupolar NMR parameters (C_Q and η), supported by GIPAW–DFT computations, provide an analytical fingerprint revealing distinct features for chemically unique Cl environments sensitive to ion mixing, dimensionality, cell volume and Cl coordinating polyhedra. Moreover, we report resolution between two nearly identical and two distinct Cl environments of 3D and 2D Cs–based lead halide perovskites, respectively. These results reveal a strategy for a routine and robust spectroscopic approach to analyze local Cl chemical environments in metal halide perovskites that can be extended broadly to other halogen containing semiconductors.

TOC GRAPHIC

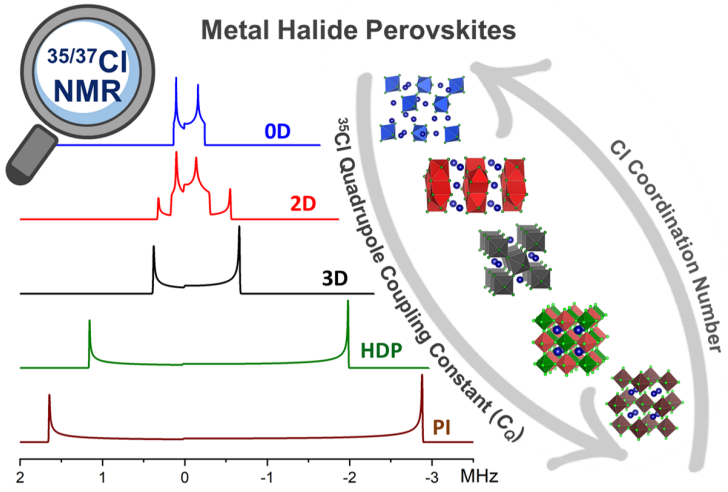

Metal halide perovskites (MHPs) are emerging as an important class of semiconducting solids that exhibit impressive optical and electrical properties.[1,2] Among them, lead halide perovskites (LHPs) are competing at the frontier of next–generation energy materials, leading in commercial advances for solar cells, LEDs, lasers, photodetectors, X–ray detectors, batteries, and photocatalytic applications.[3–9] Recently, LHPs have reached power conversion efficiencies of 25.5%,[10] surpassing that for the "gold standard" silicon solar cell. The three–dimensional (3D) LHPs are expressed using the general formula $APbX_3$ (A = Cs^+, MA^+ (methylammonium), FA^+ (formamidinium); X = $Cl^–$, $Br^–$, $I^–$), where the A–site cation resides in the cuboctahedral voids of a corner–sharing 3D network of $[PbX_6]^{4–}$ octahedra.[11] The zero–dimensional (0D) and two–dimensional (2D) LHPs are recent entrants, providing enhanced material stability, photoluminescent properties, and charge carrier recombination dynamics compared to their 3D analogues.[12–15] Cesium–based 0D and 2D LHPs can be described by the general formula Cs_4PbX_6 and $CsPb_2X_5$, respectively, where 0D Cs_4PbX_6 consists of isolated $[PbX_6]^{4–}$ octahedra surrounded by Cs^+,[16] and 2D $CsPb_2X_5$ has layers of face sharing $[PbX_8]^{6–}$ side–bicapped trigonal prisms with Cs^+ sandwiched between the layers.[17]

Environmental concerns related to lead[18] and phase instability[19] remain as commercialization challenges for LHP–based photovoltaic technologies. Inevitably, group 14 cousin materials, viz., tin and germanium halide perovskites (GHPs) are gaining further attention in the search for lead–free alternatives,[20–22] while halide double perovskites (HDPs) $[A_2B'(III)B''(I)X_6]$ consisting of corner–sharing alternate $[B'(III)X_6]^{3–}$ and $[B''(I)X_6]^{5–}$ octahedra with A–site cations residing in the cuboctahedral voids have shown improved ambient stability, excellent bandgap tunability and appealing light–emission properties.[23–25] Additionally, perovskite–inspired $A_2B(IV)X_6$ (B = Sn^{4+}, Pd^{4+}) compounds, being air–stable and environment–friendly with tailorable optoelectronic capabilities, may provide an alternative direction.[26,27] Their structure (cubic, $Fm\bar{3}m$) can be described as an ABX_3 perovskite structure with every other B–site removed. The crystal structures of several MHPs studied here are shown in Figure 1.

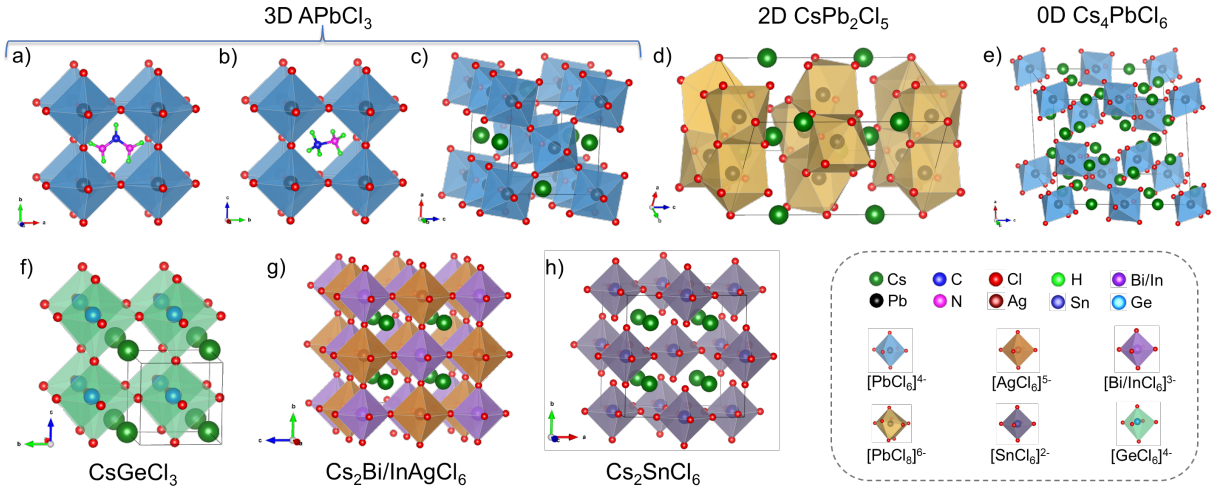

Figure 1. Crystallographic structures of lead–based 3D (a) $FAPbCl_3$, (b) $MAPbCl_3$, (c) $CsPbCl_3$, 2D (d) $CsPb_2Cl_5$, and 0D (e) Cs_4PbCl_6; (f) $CsGeCl_3$, (g) $Cs_2B'AgCl_6$ (B' = Bi or In), and (h) Cs_2SnCl_6.

Though standard characterization tools, such as diffraction techniques, are traditionally used to characterize the average long–range structures of MHPs, complementary techniques are often needed to provide further insight into local structure, vacancies, dynamics, and nanodomains.[28–30] Solid–state nuclear magnetic resonance (NMR) spectroscopy is a robust analytical method that may be used to inform on short– to medium–range structure and ion dynamics which has been shown to be a highly sensitive probe to understand the structure–property relationships displayed by MHPs.[31–35] Typically, all the constituents of MHPs have sufficiently abundant and NMR–sensitive isotopes,[34] which makes them perfect candidates for NMR analyses. Among all NMR–active nuclei in Cs–based MHPs, ^{133}Cs (nuclear spin, $I = 7/2$, quadrupolar ($I > 1/2$) but with a small quadrupole moment such that quadrupolar effects are negligible) and ^{207}Pb ($I = 1/2$) are the most intensely studied because of their relative accessibility compared to more difficult nuclei, and have contributed significantly to understanding of phase transitions,[36,37] chemical exchange reactions,[38,39] and phase segregation.[40,41] On the other hand, quadrupolar halogen nuclei ($^{35/37}$Cl, $^{79/81}$Br, ^{127}I) are extremely useful in characterizing unique chemical environments, however challenging as resolution and sensitivity is often hampered due to second–order quadrupolar broadened lineshapes.[42] The resulting quadrupolar interactions can be described by the nuclear quadrupole coupling constant (C_Q) and the asymmetry parameter (η). Recent halogen NMR and nuclear quadrupolar resonance (NQR) studies have demonstrated their utility in probing chemical structure and dynamics in solids.[34,35,42–47] Amidst the quadrupolar halogen nuclei, ^{35}Cl has a moderate quadrupole moment (Q_m) and high natural abundance (N.A.), making it a less challenging halogen nucleus for NMR studies compared to $^{79/81}$Br and ^{127}I (Table 1). While ^{37}Cl is complementary to ^{35}Cl, it is more challenging due to its lower gyromagnetic ratio and N.A.[42,45] This approach is lending support to further expansion of the NMR toolbox into these exotic NMR active nuclei, as even ^{73}Ge NMR spectroscopy has been shown to provide sensitivity of the octahedral distortion in $CsGeX_3$ (X = Cl, Br, I) perovskites.[48]

Table 1. Comparison of NMR properties of the quadrupolar ($I > 1/2$) halogen nuclei.[42]

Halogen Nucleus	I	N.A. (%)	Q_m (mb)	Ξ / %
^{35}Cl	3/2	75.78	−81.65	9.79
^{37}Cl	3/2	24.22	−64. 35	8.15
^{79}Br	3/2	50.69	313.0	25.0
^{81}Br	3/2	49.31	261.5	27.0
^{127}I	5/2	100.0	−696.0	20.0

In this letter, we determine unique ^{35}Cl (and ^{37}Cl for $CsPbCl_3$) quadrupolar NMR parameters for leading hybrid/inorganic and multidimensional metal halide perovskites, double perovskites, and perovskite–inspired materials. We also demonstrate that rapid acquisition (~30 min) of wideline NMR spectra is efficient and practical. We further discuss the highly receptive nature of ^{35}Cl NMR spectroscopy, making it suitable to elucidate distinct Cl chemical environments that are sensitive to their polyhedron geometry and coordination. In addition, we discuss the practicality of resolving multiple Cl environments and detecting low Cl concentrations (< 5%). Lastly, we demonstrate that a quantum chemical computational approach using gauge–including projector augmented waves[49] assisted density functional theory (GIPAW–DFT) reasonably predicts the ^{35}Cl quadrupolar parameters making it a useful complementary technique.

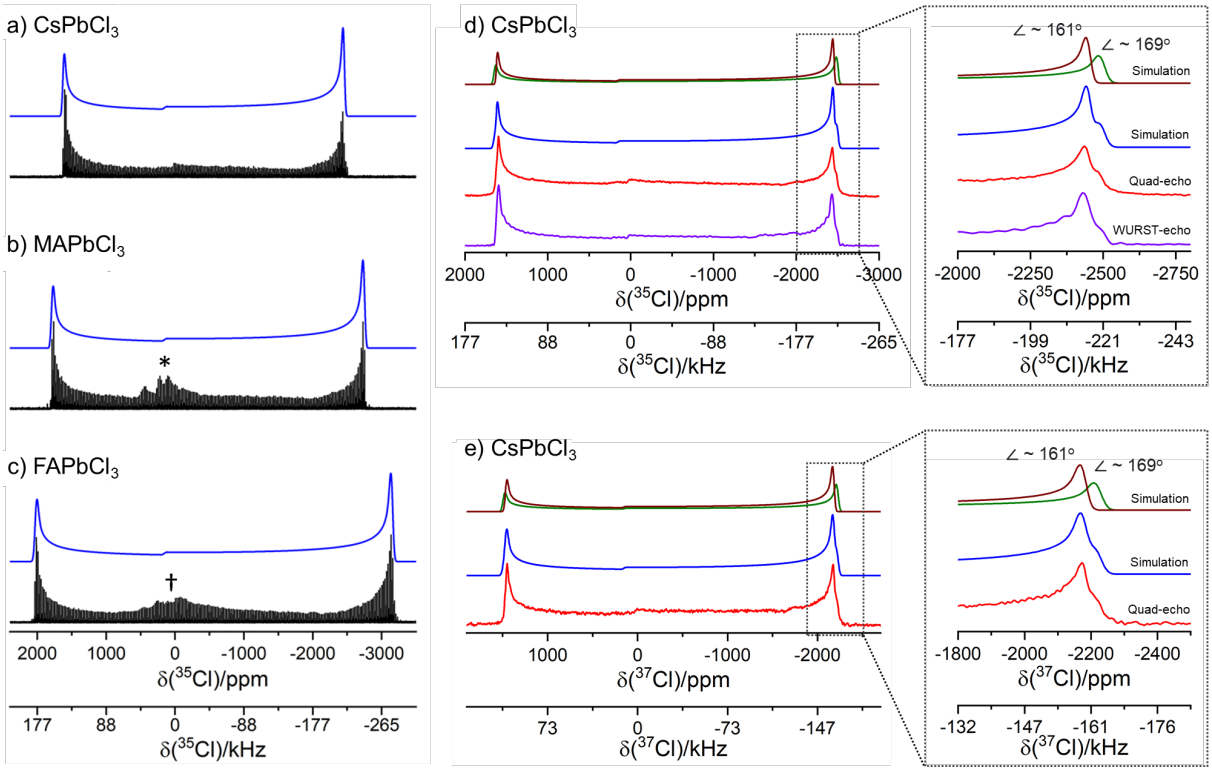

Figure 2. Non–spinning $^{35/37}$Cl NMR spectra of 3D LHPs acquired at 21.1 T at room temperature. (a) Experimental WURST–CPMG (black) and simulated (blue) ^{35}Cl NMR spectra of 3D (a) $CsPbCl_3$, and hybrid (b) $MAPbCl_3$ and (c) $FAPbCl_3$. The asterisk (*) and the dagger (†) denote the presence of $PbCl_2$ and an unidentified impurity in $MAPbCl_3$ and $FAPbCl_3$, respectively. (d) WURST–echo (violet) and quadrupolar–echo (red) ^{35}Cl NMR spectra of $CsPbCl_3$ showing resolution between two nearly identical Cl sites with slightly different Pb–Cl–Pb bond angles (∠); individual simulations of the ∠ ~ 161° (brown) and 169° (green) sites are shown above the overall simulated spectra (blue), and an enlarged view of the highlighted low–frequency shoulder is displayed. (e) Experimental quadrupolar–echo (red) and simulated (blue) ^{37}Cl NMR spectra of $CsPbCl_3$ displaying resolution between the previously mentioned Cl sites, with the corresponding simulations shown with the assignments of ∠ ~ 161° and 169° sites indicated in the figure ((brown and green, respectively). The highlighted low–frequency shoulder is enlarged.

Non–spinning ^{35}Cl NMR spectra of 3D $APbCl_3$ (A = Cs^+, MA^+, and FA^+) at 21.1 T, shown in Figure 2, display second–order quadrupolar–broadened line shapes due to the

distinct two−coordinate linear or near−linear Cl chemical environments present in these materials. The hybrid species $MAPbCl_3$ was synthesized using two synthetic routes, inverse temperature crystallization (ITC) and mechanochemical synthesis (MCS) (Figure S1a). All other bulk LHPs were prepared by MCS, and their NMR parameters are discussed here. $MAPbCl_3$ crystallizes in a cubic space group $Pm\bar{3}m$ (Figure S1a), with each Cl atom covalently bonded[50] with two Pb atoms in a collinear geometry.[51] The ^{35}Cl NMR spectrum of $MAPbCl_3$ (ITC) at 7.05 T was acquired using a Hahn−echo[52] with 13 variable offset cumulative spectra (VOCS)[53] steps (7.5 h/step) as well as a wide−band, uniform rate, and smooth truncation Carr−Purcell−Meiboom−Gill (WURST−CPMG)[54,55] pulse sequence with five VOCS steps (25 min/step) which offered a ∼47−fold savings in time (Figure S4). Parameters of $MAPbCl_3$ (MCS), extracted from the ^{35}Cl WURST−CPMG spectrum, were C_Q = 16.34 MHz, η = 0, and isotropic chemical shift (δ_{iso}) of 155 ppm. Likewise, $FAPbCl_3$, which is isostructural (Figure S1a) with a slightly larger unit cell volume[56] due to the larger FA^+ cation, has experimentally determined parameters of C_Q = 17.46 MHz, η = 0, and δ_{iso} = 160 ppm. The effect of A−site mixing was investigated by acquiring a ^{35}Cl WURST−CPMG spectrum of $FA_{0.50}MA_{0.50}PbCl_3$ (Figure S1a) at 7.05 T, and a C_Q = 16.55 MHz, η = 0, and δ_{iso} = 200 ppm were determined (Figure S5f). The stable $CsPbCl_3$ assumes a lower−symmetry orthorhombic structure (*Pnma*) (Figure S1b) with Cl atoms coordinated to two lead atoms in two different non−collinear geometries (Pb−Cl−Pb bond angles, ∠ of ∼161° and 169°, with a similar Pb−Cl bond distance of ∼2.8 Å).[57] The WURST−CPMG spectrum fails to resolve these two slightly different Cl environments and the average NMR parameters for the observed ^{35}Cl signal are C_Q = 15.60 MHz, η = 0, and δ_{iso} = 155 ppm (Figure 2a). Utilizing a ^{35}Cl WURST−echo[55] and quadrupolar−echo[58,59] experiment allowed us to resolve two nearly identical Cl sites with similar parameters η = 0 and δ_{iso} = 150 ppm, and C_Q = 15.57 and 15.71 MHz for the ∠ ∼161° and 169° environments, respectively (Figure 2d), supported by GIPAW−DFT computations. This observation was confirmed in a quadrupolar−echo experiment using ^{37}Cl NMR. The two Cl sites were resolved with C_Q = 12.27 and 12.38 MHz for ∠ ∼161° and 169°, respectively, having the same η = 0 and δ_{iso} = 150 ppm (Figure 2e). The 1.27−fold reduction in the quadrupole coupling constant for both ^{37}Cl sites is consistent with the ratio of their respective quadrupolar moments (Table 1). To obtain resolved spectra efficiently, one need not obtain the full spectrum using an echo technique as shown here. Having determined the positions of the horns in these spectra via WURST−CPMG, higher resolution spectra of just these two regions can be acquired using an echo technique. The results obtained for $CsPbCl_3$ are comparable with the recent study by Piveteau *et al.* where bulk $CsPbCl_3$ (monoclinic, $P2_1/m$) was found to have C_Q = 15.48 MHz and η = 0.[43] These three results make it apparent that all these structures contain axially symmetric Cl electric field gradient (EFG) tensors where V_{ZZ} is aligned along the direction of Pb−Cl bonds and $CsPbCl_3$ has the smallest C_Q. In fact, the formula unit cell volume (V/Z) shrinks from $FAPbCl_3$ > $FA_{0.50}MA_{0.50}PbCl_3$ (Table S5) > $MAPbCl_3$ > $CsPbCl_3$, influencing the EFG about Cl, whereby the associated C_Q decreases in a near linear (R^2 ∼ 0.9, Figure S2) relationship, suggestive of a secondary effect on the magnitude of the quadrupole

coupling, *vide infra*. In addition, the NMR spectra of these 3D LHPs were also recorded at a lower magnetic field of 7.05 T for comparative analysis (Figure S5 and S6).

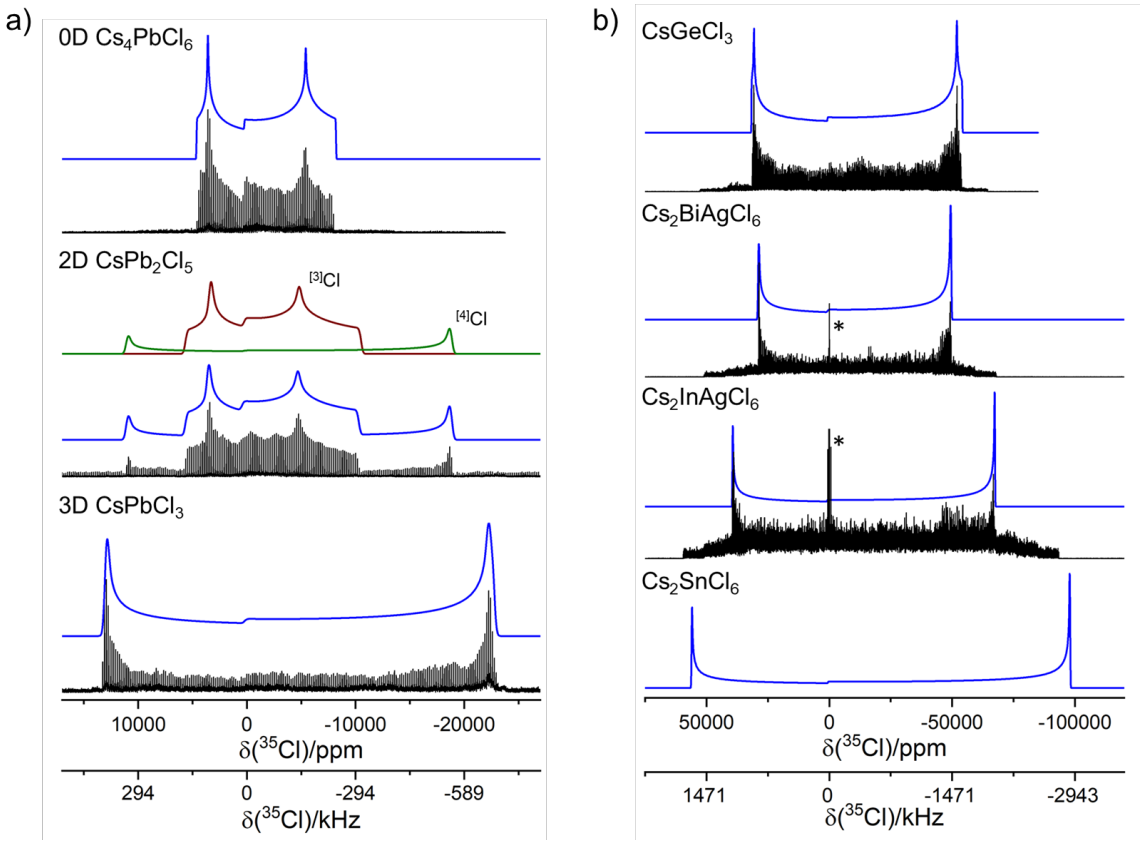

Figure 3. Experimental (black) and simulated (blue) non–spinning ^{35}Cl NMR spectra using the WURST–CPMG pulse sequence acquired at 7.05 T and room temperature. Lead–based (a) 0D Cs_4PbCl_6 (top), 2D $CsPb_2Cl_5$ (middle), and 3D $CsPbCl_3$ (bottom). The individual simulations for two different Cl environments in $CsPb_2Cl_5$ are shown above the simulated spectra for three–coordinate Cl ($^{[3]}$Cl in brown) and four–coordinate Cl ($^{[4]}$Cl in green). Lead–free (b) $CsGeCl_3$ (top), $Cs_2BiAgCl_6$ and $Cs_2InAgCl_6$ (middle), and Cs_2SnCl_6 (bottom). The asterisks (*) in (b) denote signals from an unidentified source.

Extending beyond the 3D LHPs, Figure 3a shows the non–spinning ^{35}Cl NMR spectra acquired at 7.05 T of the 0D and 2D non–hybrid LHPs, found in trigonal ($R\bar{3}c$)[60] and tetragonal ($I4/mcm$)[17] crystal symmetries (Figure S1b), respectively. The 0D Cs_4PbCl_6 perovskite has Cl atoms enclosed within a distorted Cs_5Pb quasi–octahedron[60] with the smallest ^{35}Cl quadrupole coupling constant (C_Q = 8.50 MHz) within this family of compounds, with η = 0.20 and δ_{iso} = 150 ppm (Figure 3a). The two distinct environments around Cl atoms, viz., three–coordinate $ClPb_3$ ($^{[3]}$Cl) and square planar $ClPb_4$ ($^{[4]}$Cl)[17] are clearly resolved at moderate (Figure 3a) and high (Figure S6d) magnetic fields with assignments supported by GIPAW–DFT computations. The $^{[4]}$Cl in a planar environment has a C_Q = 14.10 MHz, η = 0, and δ_{iso} = 190 ppm, while a decrease in the local coordination environment to $^{[3]}$Cl in three–coordinate geometry yields NMR parameters of C_Q = 9.00 MHz, η = 0.40 and δ_{iso} = 170 ppm. This decrease is attributed to the increased local symmetry about the Cl. A comparison of the NMR spectra recorded at 21.1 and 7.05 T for the low dimensional LHPs is shown in Figures S5 and S6. The unique

NMR parameters for the LHPs with different dimensions (above) warrant a closer look into other perovskite and perovskite–like metal chlorides.

To extend beyond lead–based perovskites, the chlorine environments of the GHP $CsGeCl_3$, and HDPs $Cs_2BiAgCl_6$ and $Cs_2InAgCl_6$ (Figure S1a) were studied via ^{35}Cl NMR spectroscopy (Figure 3b). The non–collinear geometry around the Cl atoms in $CsGeCl_3$ (rhombohedral, $R3m$)[61] with a Ge–Cl–Ge bond angle ~173° gives rise to an asymmetry parameter, η = 0.02, with a larger C_Q = 23.65 MHz and a sizeable change in the isotropic chemical shift (δ_{iso} = 850 ppm). In the case of the HDPs, both $Cs_2BiAgCl_6$ and $Cs_2InAgCl_6$ (cubic, $Fm\bar{3}m$) have linear Cl environments (η = 0) with Ag–Cl–Bi[62] or Ag–Cl–In[63] coordination. The replacement of the B–site cation with a combination of B' (Bi^{3+} or In^{3+}) and B" (Ag^+) cations in $Cs_2BiAgCl_6$ and $Cs_2InAgCl_6$ results in a significant impact on the ^{35}Cl NMR spectra with δ_{iso} values increasing to 550 and 950 ppm, respectively; deviation from linear symmetry results in increased C_Q values to 22.85 and 26.65 MHz, respectively. These results expand the Cl quadrupole coupling constants for two–coordinate linear (or near–linear) Cl species ranging here between 15 and 27 MHz depending on the medium–range B–site structure. The perovskite–inspired Cs_2SnCl_6 (cubic, $Fm\bar{3}m$) compound[64] has Cl atoms that are singly coordinated to Sn, resulting in the largest ^{35}Cl C_Q of 32 MHz (η = 0, δ_{iso} = 560 ppm) reported in this study (Figure S8).[35]

Table 2. Experimental and GIPAW–DFT computed ^{35}Cl NMR parameters of metal halide compunds.

Compound	CIF Ref.	CN	C_Q[a,b] (MHz)		η[b]		δ_{iso}[b] (ppm)	
			|Expt.|	DFT	Expt.	DFT	Expt.	DFT
Cs_2SnCl_6	[64]	1	32.0(3)[c]	−33.54	0.00[c]	0.00	560(20)[c]	447
$Cs_2InAgCl_6$	[62]	2	26.65(7)	−29.02	0.00(1)	0.00	950(150)	135
$Cs_2BiAgCl_6$	[63]	2	22.85(6)	−25.34	0.00(1)	0.00	550(120)	101
$CsGeCl_3$	[61]	2	23.65(6)	−25.30	0.02(1)	0.02	850(150)	207
$FAPbCl_3$	[56]	2	17.46(5)	−18.47	0.00(1)	0.30	160(15)	134
$MAPbCl_3$	[51]	2	16.34(6)	−18.24	0.00(1)	0.18	155(10)	140
$CsPbCl_3$	[57]	2	15.57(4)	−16.52	0.00(1)	0.01	150(10)	126
		2	15.71(3)	−16.92	0.00(1)	0.00	150(10)	120
$CsPb_2Cl_5$	[17]	3	9.00(7)	−8.59	0.40(2)	0.38	170(15)	190
		4	14.10(5)	15.34	0.00(1)	0.00	190(15)	244
Cs_4PbCl_6	[60]	6	8.50(6)	−8.92	0.20(2)	0.18	150(10)	142
CsCl (ref.)	[65]	8	0.00(1)	0.00	0.00(1)	0.00	114(1)	114

[a]Sign of C_Q were not determined experimentally. [b]Error representation is given as, e.g., 17.46 ± 0.05 MHz as 17.46(5) ppm. [c]Reference.[35]

Unlike past NMR studies on the B–sites of Pb and Sn[39,64–67] where chemical shift ranges correspond to distinct coordination geometries for these I = 1/2 nuclei, the ^{35}Cl chemical shifts of LHPs are rather crowded within a 40 ppm range. Together with the fact that each NMR signal spans thousands of ppm, this makes it nearly impossible to distinguish between multiple signals. It is therefore impractical to assess structural changes based on δ_{iso} alone. However, the ^{35}Cl quadrupolar parameters (C_Q and η) are

distinct for each compound (multidimensional LHPs, GHP, HDPS, PI) revealing that the unique EFG for each Cl site may be used to elucidate its unique coordination environment and geometry. Furthermore, while we are aware that overlap between the C_Q values for n−dimensional (n = 0, 2 and 3) LHPs can occur, discerning these unique sites in mixtures may be overcome by collecting and analyzing NMR spectra acquired at multiple−field strengths (Figure S7) or using both ^{35}Cl and ^{37}Cl probing nuclei (Figure 2).

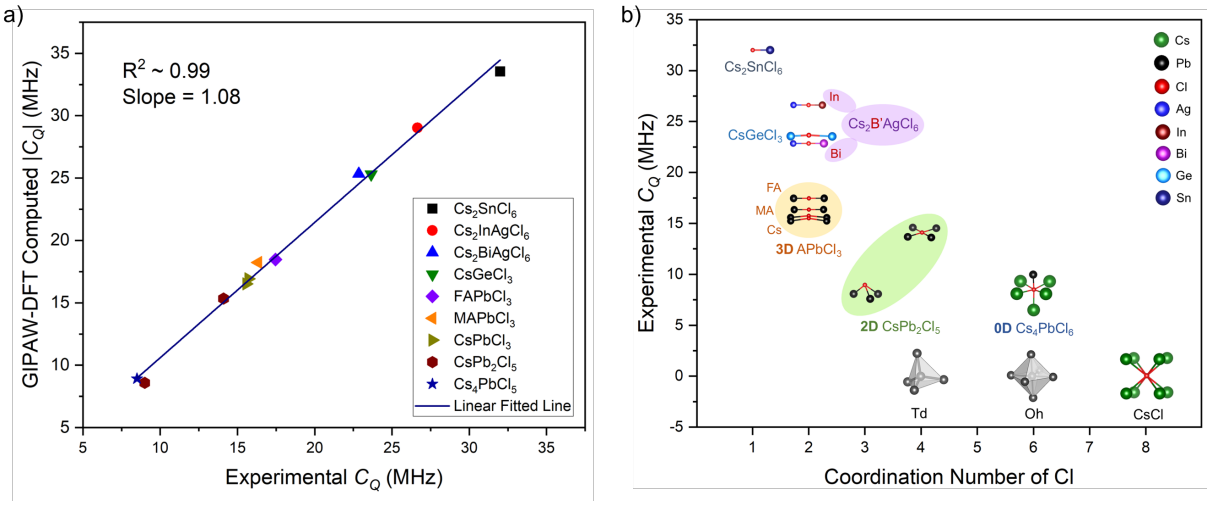

Figure 4. (a) Comparison of the experimental and GIPAW−DFT computed ^{35}Cl C_Q values for MHPs listed in Table 2. (b) Experimental C_Q values for distinct ^{35}Cl chemical polyhedra of the samples with different coordination numbers and symmetry. The highly symmetric tetrahedral (T_d) and octahedral (O_h) geometry with C_Q = 0 MHz are displayed as reference.

A series of quantum chemical computations using GIPAW−DFT were performed starting from their corresponding crystallographic information files (CIF) to assess the effectiveness of computing $^{35/37}$Cl NMR parameters in MHPs (Table 2). An area where further research efforts are needed, as we build a training set here, is to establish a predictive tool to screen NMR/NQR parameters to identify unique solutions when exploring ion substituted materials, unique chemical environments, or vacancies. Figure 4a shows that there is good agreement for the computed $|C_Q|$ values of MHPs when compared with experiment (slope ~ 1, R^2 ~ 0.99). The computed δ_{iso} values give rise to a slope of 2.92 with an R^2 of 0.94 for multidimensional LHPs (Figure S9a) and deviates further when the δ_{iso}'s for GHP, HDPs and PI materials are considered. The agreement in the quadrupolar coupling constants reinforce the growing importance of experimental NMR and theoretical computations as complementary tools to assist our understanding of the X−site in these materials. From an *in−silico* perspective, the computed chlorine NMR parameters are sensitive to local structure and dimensionality. Furthermore, the ability to accurately calculate NQR parameters is important since the signals can be very difficult to locate. The computed η values for the two hybrid LHPs (Figure S9b) deviate from the expected trend due to insertion of fixed−position hydrogen atoms within the input files. In reality, the organic molecules occupying the A−site (FA, MA) are dynamic, which result in discrepancies in their calculated η values (Table S7 and S8).[51,56] Figure 4b shows the general trend observed between Cl coordination number and C_Q for all compounds studied here including CsCl, which has a C_Q of zero due to its spherically

symmetric Cl environment. Examination of the local Cl environment for each perovskite reveals a series of unique polyhedra, where their local coordination environment and degree of polyhedral distortion guide the magnitude of the ^{35}Cl C_Q. A similar effect has been reported for ^{23}Na NMR spectra using a point charge model, whereby the degree of deviation from spherical symmetry and coordination results in sizeable changes to C_Q.[70] The computed EFG ellipsoids around the ^{35}Cl atoms of all the perovskites are displayed in Figure S10, where the largest principal component of the EFG tensor (V_{ZZ}) for all Cl atoms is aligned along their metal–Cl bonds except for four-coordinate Cl ($^{[4]}$Cl) in $CsPb_2Cl_5$.

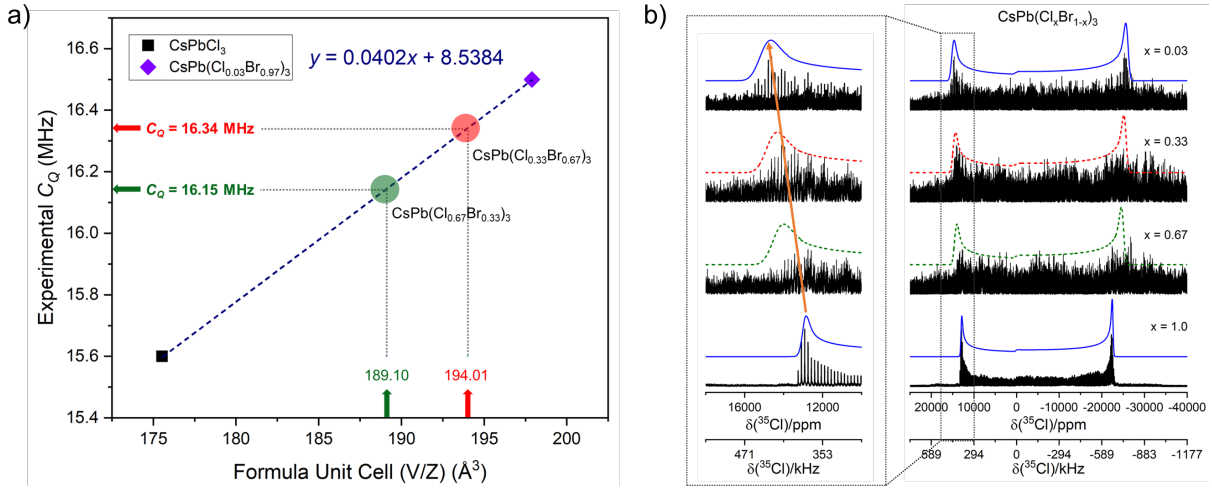

Figure 5. (a) The dependence of C_Q values with the formula unit cell volume (V/Z; Z = 4) for the mixed–halide $CsPb(Cl_xBr_{1-x})_3$ series. C_Q values for x = 0.33 and 0.67 were obtained with respect to their V/Z values from the linear equation (C_Q = 0.0402(V/Z) + 8.5384) constructed from two end points x = 0.03 and 1.0. (b) Comparison of non–spinning ^{35}Cl NMR experimental (black) and simulated (blue; for x = 0.03 and 1.0) spectra of $CsPb(Cl_xBr_{1-x})_3$ using WURST–CPMG pulse sequence recorded at 7.05 T and room temperature. The predicted C_Q values for x = 0.33 and 0.67 were used to generate the simulated spectra shown by the dotted lines in red and green, respectively, using an average δ_{iso} = 200 ppm and η = 0. The shift of the left horns towards higher frequency with a decrease in Cl concentration (x) are indicated with an arrow (orange) in the enlarged view on left in (b).

To further assess the sensitivity and utility of ultra–wideline ^{35}Cl NMR spectroscopy, the influence of Cl environments in cesium mixed–halide perovskites ($CsPb(Cl_xBr_{1-x})_3$; x = 0.03, 0.33, and 0.67) were surveyed (Figure S1b). A 3% Cl substituted–$CsPbBr_3$ compound was detectable via the ultra–wideline method at 7.05 T. Fitting the ^{35}Cl NMR spectrum revealed an experimental C_Q of 16.5 MHz (η = 0 and δ_{iso} = 250 ppm) which is an increase of ~1 MHz from the parent $CsPbCl_3$ phase (Figure 5b, top). This sensitivity test demonstrates the potential of this method in detecting Cl additives at low atomic %, such as methylammonium chloride (MACl) in MHP–based solar cells that is a common additive for improved stability and efficiency.[71] Two additional mixed–halide $CsPb(Cl_xBr_{1-x})_3$ (x = 0.33 and 0.67) perovskites were investigated and display sharp high frequency horns of the overall ^{35}Cl quadrupolar broadened central transition (Figure 5b). The poor resolution renders the challenge to determine accurate C_Q values, however it is still possible to perform a crude fit, enabling to track changes in

the quadrupolar coupling that is associated with an expansion of the unit cell, leading to changing the Cl chemical environment.

Similar to the mixed A–site cation alloys ($FA_xMA_{1-x}PbCl_3$; x = 0, 0.50, and 1.0), where the C_Q displayed a linear dependence of the volume per formula unit (V/Z) (Figure S2), the influence of V/Z on C_Q as Cl substitutions occur was examined for the $CsPb(Cl_xBr_{1-x})_3$ series. Assuming a similar linear relationship between C_Q and V/Z (C_Q = $0.0402(V/Z)$ + 8.5384) as the halide ions exchange for $CsPbCl_3$ and $CsPb(Cl_{0.03}Br_{0.97})_3$, the C_Q values of mixed–halide perovskites with Cl concentrations x = 0.33 (16.34 MHz) and x = 0.67 (16.15 MHz) were extracted with respect to their refined V/Z values (Table S5) as shown in Figure 5a. The predicted C_Q's were used to simulate the ^{35}Cl NMR spectra and show reasonable agreement with our experimental results (Figure 5b). Therefore, the dominant structural parameter driving the unique ^{35}Cl quadrupole couplings is indeed the coordination polyhedron as this would influence the electric field gradient; however, a secondary influence related to changes in the unit cell volume (contraction/expansion) further influences the quadrupole parameter as ions exchange. Unfortunately, the hybrid $MAPb(Cl_xBr_{1-x})_3$ (x = 0.25, 0.50 or 0.75) series suffers from poor sensitivity, inhibiting analysis. This unexpected outcome may be caused by shortened spin–spin relaxation (T_2) characteristics that could arise from the dynamics at the X– (halide migration) or A–site (MA/FA mobility), or both.[31,72] These dynamic considerations are inhibited within the $CsPbX_3$ series due to the smaller unit cell that results when the smaller Cs^+ resides in the A–site leading to octahedral tilting of the B–site.[15,39,72]

To conclude, we demonstrate the merit of $^{35/37}$Cl NMR spectroscopy as a fast and sensitive structural probe for characterizing unique Cl coordination geometries in various MHPs. Distinct EFG tensors for ^{35}Cl sites in these MHPs exhibit a sizeable range of C_Q values between 8.50 to 32 MHz, which have been shown to extend to over 40 MHz for other Cl–containing systems, determined using moderate field strengths.[71–75] We highlight that the range of chemical shifts of 40 ppm for LHPs is very small with respect to the experimental spectra that span thousands of ppm in these materials due to sizable second–order quadrupolar broadening, thereby making C_Q a more efficient and sensitive parameter in discriminating specific Cl chemical environments. Resolution between two nearly identical crystallographic Cl environments of 3D Cs–based lead halide perovskite using both ^{35}Cl and ^{37}Cl NMR reveals the profound capabilities of this approach to discern between two similar Cl environments. The ^{35}Cl NMR spectrum for the 2D lead halide perovskite reveals two crystallographically distinct Cl environments at moderate fields. In general, C_Q decreases with increasing Cl coordination number and is influenced by the degree of polyhedral distortion. Overlapping Cl environments may be resolved using a combination of multiple–field strengths, isotope selection, and NMR experimental methods. These methods can be further extended to materials with low Cl substitution or cation/anion modifications. Finally, the GIPAW–DFT results helped reliably estimate the quadrupolar NMR parameters in Cl–containing MHPs. This will be used to optimize experimental wideline acquisition parameters, to suggest assignments as well as to narrow the search space in NQR applications.

ASSOCIATED CONTENT

Supporting Information

Additional discussion about experimental techniques and GIPAW–DFT computations with Tables S1–S11 and Figures S1–S10 are available in the Supporting Information (PDF).

AUTHOR INFORMATION

Corresponding Author

Vladimir K. Michaelis – *Department of Chemistry, University of Alberta, Edmonton, Alberta T6G 2G2, Canada*
Email: vladimir.michaelis@ualberta.ca

Authors

Diganta Sarkar – *Department of Chemistry, University of Alberta, Edmonton, Alberta T6G 2G2, Canada*
Riley W. Hooper – *Department of Chemistry, University of Alberta, Edmonton, Alberta T6G 2G2, Canada*
Abhoy Karmakar – *Department of Chemistry, University of Alberta, Edmonton, Alberta T6G 2G2, Canada*
Amit Bhattacharya – *Department of Chemistry, University of Alberta, Edmonton, Alberta T6G 2G2, Canada*
Arkadii Pominov – *Department of Chemistry, University of Alberta, Edmonton, Alberta T6G 2G2, Canada*
Victor V. Terskikh – *Metrology, National Research Council of Canada, Ottawa, Ontario K1A 0R6, Canada*

Notes

The authors declare no competing financial interests.

ACKNOWLEDGEMENTS

We acknowledge the Natural Science and Engineering Research Council of Canada (DG and CREATE–ATUMS), Canada Research Chairs Program, Canada Foundation for Innovation and the Government of Alberta for research support. D.S. is supported by an Alberta Innovates Graduate Fellowship. R.W.H. is supported by an NSERC CGSD3, and Alberta Innovates Graduate Fellowship. Access to the 21.1 T NMR spectrometer was provided by the National Ultrahigh–Field NMR Facility for Solids (Ottawa, Canada), a national research facility funded by a consortium of Canadian Universities and managed by the National Research Council Canada (*http://nmr900.ca*). The authors thank Dylan G. Tkachuk for assistance with GIPAW–DFT computations and Yingjie He for performing an SEM measurement.

REFERENCES

(1) Zhang, W.; Eperon, G. E.; Snaith, H. J. Metal Halide Perovskites for Energy Applications. *Nat. Energy* **2016**, *1*, 1–8.

(2) Liu, X. K.; Xu, W.; Bai, S.; Jin, Y.; Wang, J.; Friend, R. H.; Gao, F. Metal Halide Perovskites for Light–Emitting Diodes. *Nat. Mater.* **2020**, *20*, 10–21.

(3) Qin, P.; Tanaka, S.; Ito, S.; Tetreault, N.; Manabe, K.; Nishino, H.; Nazeeruddin, M. K.; Grätzel, M. Inorganic Hole Conductor–Based Lead Halide Perovskite Solar Cells with 12.4% Conversion Efficiency. *Nat. Commun.* **2014**, *5*, 1–6.

(4) Song, J.; Li, J.; Li, X.; Xu, L.; Dong, Y.; Zeng, H. Quantum Dot Light–Emitting Diodes Based on Inorganic Perovskite Cesium Lead Halides ($CsPbX_3$). *Adv. Mater.* **2015**, *27*, 7162–7167.

(5) Zhu, H.; Fu, Y.; Meng, F.; Wu, X.; Gong, Z.; Ding, Q.; Gustafsson, M. V.; Trinh, M. T.; Jin, S.; Zhu, X.–Y. Lead Halide Perovskite Nanowire Lasers with Low Lasing Thresholds and High Quality Factors. *Nat. Mater.* **2015**, *14*, 636–642.

(6) Zhou, H.; Song, Z.; Grice, C. R.; Chen, C.; Yang, X.; Wang, H.; Yan, Y. Pressure–Assisted Annealing Strategy for High–Performance Self–Powered All–Inorganic Perovskite Microcrystal Photodetectors. *J. Phys. Chem. Lett.* **2018**, *9*, 4714–4719.

(7) Yakunin, S.; Sytnyk, M.; Kriegner, D.; Shrestha, S.; Richter, M.; Matt, G. J.; Azimi, H.; Brabec, C. J.; Stangl, J.; Kovalenko, M. V.; Heiss, W. Detection of X–Ray Photons by Solution–Processed Lead Halide Perovskites. *Nat. Photonics* **2015**, *9*, 444–449.

(8) Zhang, L.; Miao, J.; Li, J.; Li, Q. Halide Perovskite Materials for Energy Storage Applications. *Adv. Funct. Mater.* **2020**, *30*, 2003653.

(9) Zhu, X.; Lin, Y.; San Martin, J.; Sun, Y.; Zhu, D.; Yan, Y. Lead Halide Perovskites for Photocatalytic Organic Synthesis. *Nat. Commun.* **2019**, *10*, 1–10.

(10) National Renewable Energy Laboratory (NREL). Best Research–Cell Efficiency Chart https://www.nrel.gov/pv/assets/pdfs/best–research–cell–efficiencies–rev210726.pdf (accessed Oct 8, 2021).

(11) Kovalenko, M. V.; Protesescu, L.; Bodnarchuk, M. I. Properties and Potential Optoelectronic Applications of Lead Halide Perovskite Nanocrystals. *Science* **2017**, *358*, 745–750.

(12) Saidaminov, M. I.; Almutlaq, J.; Sarmah, S.; Dursun, I.; Zhumekenov, A. A.; Begum, R.; Pan, J.; Cho, N.; Mohammed, O. F.; Bakr, O. M. Pure Cs_4PbBr_6: Highly Luminescent Zero–Dimensional Perovskite Solids. *ACS Energy Lett.* **2016**, *1*, 840–845.

(13) Bao, J.; Hadjiev, V. G. Origin of Luminescent Centers and Edge States in Low–Dimensional Lead Halide Perovskites: Controversies, Challenges and Instructive Approaches. *Nano–Micro Lett.* **2019**, *11*, 1–18.

(14) Cho, J.; Dubose, J. T.; Kamat, P. V. Charge Carrier Recombination Dynamics of Two–Dimensional Lead Halide Perovskites. *J. Phys. Chem. Lett.* **2020**, *11*, 2021.

(15) Karmakar, A.; Dodd, M. S.; Zhang, X.; Oakley, M. S.; Klobukowski, M.; Michaelis, V. K. Mechanochemical Synthesis of 0D and 3D Cesium Lead Mixed Halide Perovskites. *Chem. Commun.* **2019**, *55*, 5079–5082.

(16) Akkerman, Q. A.; Abdelhady, A. L.; Manna, L. Zero–Dimensional Cesium Lead Halides: History, Properties, and Challenges. *J. Phys. Chem. Lett.* **2018**, *9*, 2326–2337.

(17) Chen, Y.; Molokeev, M. S.; Atuchin, V. V; Reshak, A. H.; Auluck, S.; Alahmed, Z. A.; Xia, Z. Synthesis, Crystal Structure, and Optical Gap of Two–Dimensional Halide Solid Solutions $CsPb_2(Cl_{1-x}Br_x)_5$. *Inorg. Chem.* **2018**, *57*, 9.

(18) Li, J.; Cao, H. L.; Jiao, W. Bin; Wang, Q.; Wei, M.; Cantone, I.; Lü, J.; Abate, A. Biological Impact of Lead from Halide Perovskites Reveals the Risk of Introducing a Safe Threshold. *Nat. Commun.* **2020**, *11*, 1–5.

(19) Berhe, T. A.; Su, W. N.; Chen, C. H.; Pan, C. J.; Cheng, J. H.; Chen, H. M.; Tsai, M. C.; Chen, L. Y.; Dubale, A. A.; Hwang, B. J. Organometal Halide Perovskite Solar Cells: Degradation and Stability. *Energy Environ. Sci.* **2016**, *9*, 323–356.

(20) Xi, J.; Loi, M. A. The Fascinating Properties of Tin–Alloyed Halide Perovskites. *ACS Energy Lett.* **2021**, *6*, 1803–1810.

(21) Schileo, G.; Grancini, G. Lead or No Lead? Availability, Toxicity, Sustainability and

Environmental Impact of Lead–Free Perovskite Solar Cells. *J. Mater. Chem. C* **2021**, *9*, 67–76.
(22) Ito, N.; Kamarudin, M. A.; Hirotani, D.; Zhang, Y.; Shen, Q.; Ogomi, Y.; Iikubo, S.; Minemoto, T.; Yoshino, K.; Hayase, S. Mixed Sn–Ge Perovskite for Enhanced Perovskite Solar Cell Performance in Air. *J. Phys. Chem. Lett.* **2018**, *9*, 1682–1688.
(23) Slavney, A. H.; Hu, T.; Lindenberg, A. M.; Karunadasa, H. I. A Bismuth–Halide Double Perovskite with Long Carrier Recombination Lifetime for Photovoltaic Applications. *J. Am. Chem. Soc.* **2016**, *138*, 2138–2141.
(24) Karmakar, A.; Dodd, M. S.; Agnihotri, S.; Ravera, E.; Michaelis, V. K. Cu(II)–Doped $Cs_2SbAgCl_6$ Double Perovskite: A Lead–Free, Low–Bandgap Material. *Chem. Mater.* **2018**, *30*, 8280–8290.
(25) Karmakar, A.; Bernard, G. M.; Meldrum, A.; Oliynyk, A. O.; Michaelis, V. K. Tailorable Indirect to Direct Band–Gap Double Perovskites with Bright White–Light Emission: Decoding Chemical Structure Using Solid–State NMR. *J. Am. Chem. Soc.* **2020**, *142*, 10780–10793.
(26) Lee, B.; Stoumpos, C. C.; Zhou, N.; Hao, F.; Malliakas, C.; Yeh, C. Y.; Marks, T. J.; Kanatzidis, M. G.; Chang, R. P. H. Air–Stable Molecular Semiconducting Iodosalts for Solar Cell Applications: Cs_2SnI_6 as a Hole Conductor. *J. Am. Chem. Soc.* **2014**, *136*, 15379–15385.
(27) Sakai, N.; Haghighirad, A. A.; Filip, M. R.; Nayak, P. K.; Nayak, S.; Ramadan, A.; Wang, Z.; Giustino, F.; Snaith, H. J. Solution–Processed Cesium Hexabromopalladate(IV), Cs_2PdBr_6, for Optoelectronic Applications. *J. Am. Chem. Soc.* **2017**, *139*, 6030–6033.
(28) Kubicki, D. J.; Stranks, S. D.; Grey, C. P.; Emsley, L. NMR Spectroscopy Probes Microstructure, Dynamics and Doping of Metal Halide Perovskites. *Nat. Rev. Chem.* **2021**, *5*, 624–645.
(29) Moudrakovski, I. L. Local Dynamics in Hybrid Perovskites by Solid–State NMR. *Annu. Reports NMR Spectrosc.* **2021**, *102*, 269–341.
(30) Bernard, G. M.; Karmakar, A.; Michaelis, V. K. Solid–State NMR Studies of Halide Perovskite Materials with Photoconversion Potential. *Ref. Modul. Chem. Mol. Sci. Chem. Eng.* **2021**.
(31) Bernard, G. M.; Wasylishen, R. E.; Ratcliffe, C. I.; Terskikh, V.; Wu, Q.; Buriak, J. M.; Hauger, T. Methylammonium Cation Dynamics in Methylammonium Lead Halide Perovskites: A Solid–State NMR Perspective. *J. Phys. Chem. A* **2018**, *122*, 1560–1573.
(32) Kubicki, D. J.; Prochowicz, D.; Hofstetter, A.; Péchy, P.; Zakeeruddin, S. M.; Grätzel, M.; Emsley, L. Cation Dynamics in Mixed–Cation $(MA)_x(FA)_{1-x}PbI_3$ Hybrid Perovskites from Solid–State NMR. *J. Am. Chem. Soc.* **2017**, *139*, 10055–10061.
(33) Franssen, W. M. J.; Es, S. G. D. van; Dervişoğlu, R.; Wijs, G. A. de; Kentgens, A. P. M. Symmetry, Dynamics, and Defects in Methylammonium Lead Halide Perovskites. *J. Phys. Chem. Lett.* **2016**, *8*, 61–66.
(34) Piveteau, L.; Morad, V.; Kovalenko, M. V. Solid–State NMR and NQR Spectroscopy of Lead–Halide Perovskite Materials. *J. Am. Chem. Soc.* **2020**, *142*, 19413–19437.
(35) Karmakar, A.; Mukhopadhyay, S.; Gachod, P. G. B.; Mora–Gomez, V. A.; Bernard, G. M.; Brown, A.; Michaelis, V. K. Uncovering Halogen Mixing and Octahedral Dynamics in Cs_2SnX_6 by Multinuclear Magnetic Resonance Spectroscopy. *Chem. Mater.* **2021**, *33*, 6078–6090.
(36) Lim, A. R.; Jeong, S. Y. Ferroelastic Phase Transition and Twin Structure by ^{133}Cs NMR in a $CsPbCl_3$ Single Crystal. *Phys. B Condens. Matter* **2001**, *304*, 79–85.
(37) Ae, R. L.; In, G. K. Phase Transition Study by Using ^{133}Cs and ^{207}Pb Nuclear Magnetic Resonance in a $CsPbCl_3$ Single Crystal. *J. Phys. Soc. Japan* **2013**, *73*, 475–479.
(38) Karmakar, A.; Askar, A. M.; Bernard, G. M.; Terskikh, V. V.; Ha, M.; Patel, S.; Shankar, K.; Michaelis, V. K. Mechanochemical Synthesis of Methylammonium Lead Mixed–Halide Perovskites: Unraveling the Solid–Solution Behavior Using Solid–State NMR. *Chem. Mater.* **2018**, *30*, 2309–2321.
(39) Askar, A. M.; Karmakar, A.; Bernard, G. M.; Ha, M.; Terskikh, V. V.; Wiltshire, B. D.; Patel, S.; Fleet, J.; Shankar, K.; Michaelis, V. K. Composition–Tunable Formamidinium Lead Mixed Halide Perovskites via Solvent–Free Mechanochemical Synthesis: Decoding the Pb Environments Using Solid–State NMR Spectroscopy. *J. Phys. Chem. Lett.* **2018**, *9*, 2671–2677.

(40) Kubicki, D. J.; Prochowicz, D.; Hofstetter, A.; Zakeeruddin, S. M.; Grätzel, M.; Emsley, L. Phase Segregation in Cs–, Rb– and K–Doped Mixed–Cation $(MA)_x(FA)_{1-x}PbI_3$ Hybrid Perovskites from Solid–State NMR. *J. Am. Chem. Soc.* **2017**, *139*, 14173–14180.
(41) Kubicki, D. J.; Prochowicz, D.; Hofstetter, A.; Zakeeruddin, S. M.; Grätzel, M.; Emsley, L. Phase Segregation in Potassium–Doped Lead Halide Perovskites from ^{39}K Solid–State NMR at 21.1 T. *J. Am. Chem. Soc.* **2018**, *140*, 7232–7238.
(42) Szell, P. M. J.; Bryce, D. L. Recent Advances in Chlorine, Bromine, and Iodine Solid–State NMR Spectroscopy. *Annu. Reports NMR Spectrosc.* **2020**, *100*, 97–152.
(43) Piveteau, L.; Aebli, M.; Yazdani, N.; Millen, M.; Korosec, L.; Krieg, F.; Benin, B. M.; Morad, V.; Piveteau, C.; Shiroka, T.; Comas–Vives, A.; Copéret, C.; Lindenberg, A. M.; Wood, V.; Verel, R.; Kovalenko, M. V. Bulk and Nanocrystalline Cesium Lead–Halide Perovskites as Seen by Halide Magnetic Resonance. *ACS Cent. Sci.* **2020**, *6*, 1138–1149.
(44) Aebli, M.; Porenta, N.; Aregger, N.; Kovalenko, M. V. Local Structure of Multinary Hybrid Lead Halide Perovskites Investigated by Nuclear Quadrupole Resonance Spectroscopy. *Chem. Mater.* **2021**, *33*, 6965–6973.
(45) Szell, P. M. J.; Bryce, D. L. Solid–State Nuclear Magnetic Resonance and Nuclear Quadrupole Resonance as Complementary Tools to Study Quadrupolar Nuclei in Solids. *Concepts Magn. Reson. Part A Bridg. Educ. Res.* **2016**, *45A*.
(46) Perras, F. A.; Bryce, D. L.; Perras, F. A.; Bryce, D. L. Direct Investigation of Covalently Bound Chlorine in Organic Compounds by Solid–State ^{35}Cl NMR Spectroscopy and Exact Spectral Line–Shape Simulations. *Angew. Chemie Int. Ed.* **2012**, *51*, 4227–4230.
(47) Szell, P. M. J.; Bryce, D. L. ^{35}Cl Solid–State NMR and Computational Study of Chlorine Halogen Bond Donors in Single–Component Crystalline Chloronitriles. *J. Phys. Chem. C* **2016**, *120*, 11121–11130.
(48) Hooper, R. W.; Ni, C.; Tkachuk, D. G.; He, Y.; Terskikh, V. V.; Veinot, J. G. C.; Michaelis, V. K. Exploring Structural Nuances in Germanium Halide Perovskites Using Solid–State ^{73}Ge and ^{133}Cs NMR Spectroscopy. *J. Phys. Chem. Lett.* **2022**, *13*, 1687–1696.
(49) Pickard, C. J.; Mauri, F. All–Electron Magnetic Response with Pseudopotentials: NMR Chemical Shifts. *Phys. Rev. B* **2001**, *63*, 245101.
(50) Aebli, M.; Piveteau, L.; Nazarenko, O.; Benin, B. M.; Krieg, F.; Verel, R.; Kovalenko, M. V. Lead–Halide Scalar Couplings in ^{207}Pb NMR of $APbX_3$ Perovskites (A = Cs, Methylammonium, Formamidinium; X = Cl, Br, I). *Sci. Rep.* **2020**, *10*, 1–9.
(51) Chen, K.; Deng, X.; Goddard, R.; Tüysüz, H. Pseudomorphic Transformation of Organometal Halide Perovskite Using the Gaseous Hydrogen Halide Reaction. *Chem. Mater.* **2016**, *28*, 5530–5537.
(52) Hahn, E. L. Spin Echoes. *Phys. Rev.* **1950**, *80*, 580.
(53) Massiot, D.; Farnan, I.; Gautier, N.; Trumeau, D.; Trokiner, A.; Coutures, J. P. ^{71}Ga and ^{69}Ga Nuclear Magnetic Resonance Study of β–Ga_2O_3: Resolution of Four– and Six–Fold Coordinated Ga Sites in Static Conditions. *Solid State Nucl. Magn. Reson.* **1995**, *4*, 241–248.
(54) O'Dell, L. A.; Schurko, R. W. QCPMG Using Adiabatic Pulses for Faster Acquisition of Ultra–Wideline NMR Spectra. *Chem. Phys. Lett.* **2008**, *464*, 97–102.
(55) O'Dell, L. A. The WURST Kind of Pulses in Solid–State NMR. *Solid State Nucl. Magn. Reson.* **2013**, *55–56*, 28–41.
(56) Govinda, S.; Kore, B. P.; Swain, D.; Hossain, A.; De, C.; Row, T. N. G.; Sarma, D. D. Critical Comparison of $FAPbX_3$ and $MAPbX_3$ (X = Br and Cl): How Do They Differ? *J. Phys. Chem. C* **2018**, *122*, 13758–13766.
(57) Linaburg, M. R.; McClure, E. T.; Majher, J. D.; Woodward, P. M. $Cs_{1-x}Rb_xPbCl_3$ and $Cs_{1-x}Rb_xPbBr_3$ Solid Solutions: Understanding Octahedral Tilting in Lead Halide Perovskites. *Chem. Mater.* **2017**, *29*, 3507–3514.
(58) Weisman, I. D.; Bennett, L. H. Quadrupolar Echoes in Solids. *Phys. Rev.* **1969**, *181* (3), 1341.
(59) Davis, J. H.; Jeffrey, K. R.; Bloom, M.; Valic, M. I.; Higgs, T. P. Quadrupolar Echo Deuteron Magnetic Resonance Spectroscopy in Ordered Hydrocarbon Chains. *Chem. Phys. Lett.* **1976**, *42*, 390–394.
(60) Cenzual, K.; Gelato, L. M.; Penzo, M.; Parthé, E. Overlooked Trigonal Symmetry in Structures

Reported with Monoclinic Centred Bravais Lattices; Trigonal Description of Li_8Pb_3, PtTe, Pt_3Te_4, Pt_2Te_3, $LiFe_6Ge_4$, $LiFe_6Ge_5$, $CaGa_6Te_{10}$ and $La_{3.266}Mn_{1.1}S_6$. *Zeitschrift für Krist. – Cryst. Mater.* **1990**, *193*, 217–242.

(61) Thiele, G.; Rotter, H. W.; Schmidt, K. D. Kristallstrukturen Und Phasentransformationen von Caesiumtrihalogenogermanaten(II) $CsGeX_3$ (X = Cl, Br, I). *Zeitschrift für Anorg. und Allg. Chemie* **1987**, *545*, 148–156.

(62) McClure, E. T.; Ball, M. R.; Windl, W.; Woodward, P. M. Cs_2AgBiX_6 (X = Br, Cl): New Visible Light Absorbing, Lead–Free Halide Perovskite Semiconductors. *Chem. Mater.* **2016**, *28*, 1348–1354.

(63) Zhou, J.; Xia, Z.; Molokeev, M. S.; Zhang, X.; Peng, D.; Liu, Q. Composition Design, Optical Gap and Stability Investigations of Lead–Free Halide Double Perovskite $Cs_2AgInCl_6$. *J. Mater. Chem. A* **2017**, *5*, 15031–15037.

(64) Persson, K. Materials Data on Cs_2SnCl_6 (SG:225) by Materials Project https://materialsproject.org/materials/mp–608555/ (accessed Aug 30, 2021).

(65) Cortona, P. Direct Determination of Self–Consistent Total Energies and Charge Densities of Solids: A Study of the Cohesive Properties of the Alkali Halides. *Phys. Rev. B* **1992**, *46*, 2008.

(66) Karmakar, A.; Bhattacharya, A.; Bernard, G. M.; Mar, A.; Michaelis, V. K. Revealing the Local Sn and Pb Arrangements in $CsSn_xPb_{1-x}Br_3$ Perovskites with Solid–State NMR Spectroscopy. *ACS Mater. Lett.* **2021**, *3*, 261–267.

(67) Karmakar, A.; Bhattacharya, A.; Sarkar, D.; Bernard, G. M.; Mar, A.; Michaelis, V. K. Influence of Hidden Halogen Mobility on Local Structure of $CsSn(Cl_{1-x}Br_x)_3$ Mixed–Halide Perovskites by Solid–State NMR. *Chem. Sci.* **2021**, *12*, 3253–3263.

(68) Ha, M.; Karmakar, A.; Bernard, G. M.; Basilio, E.; Krishnamurthy, A.; Askar, A. M.; Shankar, K.; Kroeker, S.; Michaelis, V. K. Phase Evolution in Methylammonium Tin Halide Perovskites with Variable Temperature Solid–State ^{119}Sn NMR Spectroscopy. *J. Phys. Chem. C* **2020**, *124*, 15015–15027.

(69) Rosales, B. A.; Hanrahan, M. P.; Boote, B. W.; Rossini, A. J.; Smith, E. A.; Vela, J. Lead Halide Perovskites: Challenges and Opportunities in Advanced Synthesis and Spectroscopy. *ACS Energy Lett.* **2017**, *2*, 906–914.

(70) Koller, H.; Engelhardt, G.; Kentgens, A. P. M.; Sauer, J. ^{23}Na NMR Spectroscopy of Solids: Interpretation of Quadrupole Interaction Parameters and Chemical Shifts. *J. Physial Chem.* **1994**, *98*, 1544–1551.

(71) Odysseas Kosmatos, K.; Theofylaktos, L.; Giannakaki, E.; Deligiannis, D.; Konstantakou, M.; Stergiopoulos, T. Methylammonium Chloride: A Key Additive for Highly Efficient, Stable, and Up–Scalable Perovskite Solar Cells. *Energy Environ. Mater.* **2019**, *2*, 79–92.

(72) Karmakar, A.; Askar, A. M.; Bernard, G. M.; Terskikh, V. V.; Ha, M.; Patel, S.; Shankar, K.; Michaelis, V. K. Mechanochemical Synthesis of Methylammonium Lead Mixed–Halide Perovskites: Unraveling the Solid–Solution Behavior Using Solid–State NMR. *Chem. Mater.* **2018**, *30*, 2309–2321.

(73) Lucier, B. E. G.; Terskikh, V. V.; Guo, J.; Bourque, J. L.; McOnie, S. L.; Ripmeester, J. A.; Huang, Y.; Baines, K. M. Chlorine–35 Solid–State Nuclear Magnetic Resonance Spectroscopy as an Indirect Probe of the Oxidation Number of Tin in Tin Chlorides. *Inorg. Chem.* **2020**, *59*, 13651–13670.

(74) Lucier, B. E. G.; Johnston, K. E.; Xu, W.; Hanson, J. C.; Senanayake, S. D.; Yao, S.; Bourassa, M. W.; Srebro, M.; Autschbach, J.; Schurko, R. W. Unravelling the Structure of Magnus' Pink Salt. *J. Am. Chem. Soc.* **2014**, *136*, 1333–1351.

(75) Lucier, B. E. G.; Reidel, A. R.; Schurko, R. W. Multinuclear Solid–State NMR of Square–Planar Platinum Complexes — Cisplatin and Related Systems. *Can. J. Chem.* **2011**, *89*, 919–937.

(76) Rossini, A. J.; Mills, R. W.; Briscoe, G. A.; Norton, E. L.; Geier, S. J.; Hung, I.; Zheng, S.; Autschbach, J.; Schurko, R. W. Solid–State Chlorine NMR of Group IV Transition Metal Organometallic Complexes. *J. Am. Chem. Soc.* **2009**, *131*, 3317–3330.

(77) P. Chapman, R.; L. Bryce, D. Application of Multinuclear Magnetic Resonance and Gauge–Including Projector–Augmented–Wave Calculations to the Study of Solid Group 13 Chlorides. *Phys. Chem. Chem. Phys.* **2009**, *11*, 6987–6998.